Nitric acid dihydrate at ambient and high pressure: An experimental and computational study

Martin Walker,[1] Colin R. Pulham,[1] Carole A. Morrison,[1] David R. Allan,[1] and William G. Marshall[2]
[1]*School of Chemistry, University of Edinburgh, The King's Buildings, West Mains Road, Edinburgh, EH9 3JJ, United Kingdom*
[2]*ISIS Neutron Facility, Rutherford Appleton Laboratory, Chilton, Didcot, Oxon OX11 0QX, United Kingdom*
(Received 12 April 2006; published 19 June 2006)

The high pressure structural behavior of nitric acid dihydrate ($[H_3O]^+ \cdot [NO_3]^- \cdot H_2O$) has been investigated up to 3.8 GPa using single crystal x-ray diffraction and neutron powder diffraction techniques. A new structural phase has been identified above 1.33 GPa and this has been further studied by *ab initio* quantum mechanical calculations. These have guided the refinement by neutron powder diffraction.

DOI: 10.1103/PhysRevB.73.224110 PACS number(s): 61.12.−q, 61.10.Nz, 61.18.−j, 61.43.Bn

INTRODUCTION

Nitric acid (HNO_3) and hydrates of nitric acid are ubiquitous and are used or produced in many processes. As one of the major components of polar stratospheric clouds (PSCs), nitric acid is the focus of much research. During the polar winter when PSCs freeze a deep hole in the stratosphere, ozone develops. It has been hypothesized that PSCs are responsible for ozone depletion, and the hydrates of nitric acid have been identified as possible catalysts.[1] Previous studies to investigate the catalytic pathway have only considered the hydrate crystal structures that form under ambient pressure conditions.[2,3] By applying pressure, the structural behavior of a material can be systematically investigated, and any subsequent new phases obtained can be identified and characterized by diffraction methods.

Nitric acid is known to crystallize with one, two, or three water molecules in the crystallographic unit cell, and a recent report has also suggested the presence of a pentahydrate structure.[4] Several studies have been conducted on the behavior of a number of nitric acid hydrates, their phase diagrams, and the crystalline structures of their different solid phases.[5,6] This paper is the second of two reports detailing how high-pressure x-ray crystallography and quantum mechanical calculations can be combined to complete a structural investigation. In the first paper,[7] nitric acid monohydrates (NAM) were explored. In this paper, we now turn to the more complex case of nitric acid dihydrate (NAD). Of the two, NAD is the more complicated structure to generate, requiring thermal treatment to obtain a pure phase.

The x-ray structure of the nitric acid dihydrate has been reported on more recently than the monohydrate analogue. To date, two phases at ambient pressure have been described by Lebrun *et al.*[5,6] Central to the crystallography is the geometry of the $[H_5O_2]^+$ cation (known in the literature as the Zundel complex[8] or dihydronium ion). Dai *et al.*[9] reported a recent theoretical study which found a C_2 symmetry global minimum structure for this complex [Fig. 1(a), labeled type 1]. In the two ambient pressure crystal structures reported for NAD a further two conformations, also with C_2 symmetry, are observed [Figs. 1(b) and 1(c), labeled type 2 and type 3, respectively].

The low temperature (200 K) ambient pressure (phase I) structure ($P2_1/n$) can be described as noninteracting bilayers of NAD units. An extensive network of hydrogen bonding makes up each of the monolayers, which are in turn connected through a longer hydrogen bond originating from a H_2O molecule (see Fig. 2). Two forms of the dihydronium ion are present in this structure: Type 2 cations are bonded solely in the monolayers, and type 1 are responsible for the bonding between the monolayers (see Fig. 2).

Slowly raising the temperature to 225 K generates a new polymorph of NAD. The shape of the unit cell has altered such that the longest crystallographic axis has changed from *a* (phase I) to *b* (phase II); a volume increase of 1% has also occurred upon temperature increase. The crystal structure of phase II has at least one hydrogen bond along each of the crystallographic axes. This polymorph crystallizes in the same space group as phase I ($P2_1/n$) and a similar H-bonding motif can be observed, except that all layers are now held together by hydrogen bonds originating from the water molecules (four per unit cell). Once again, type 2 dihydronium ions form hydrogen bonds solely in the monolayers. However, in this phase it is type 3 ions that are responsible for the interactions between the layers (see Fig. 3).

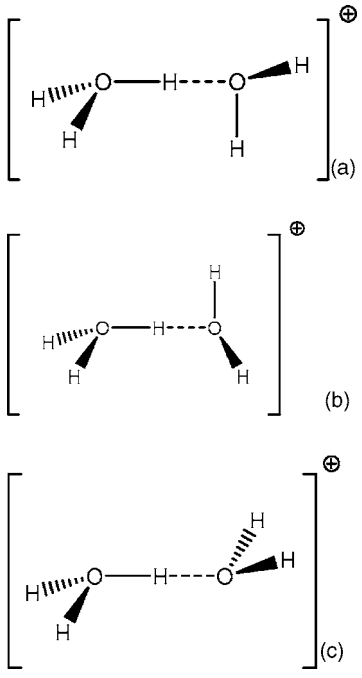

FIG. 1. The three conformations of $[H_5O_2]^+$ (a) type 1, (b) type 2, and (c) type 3.

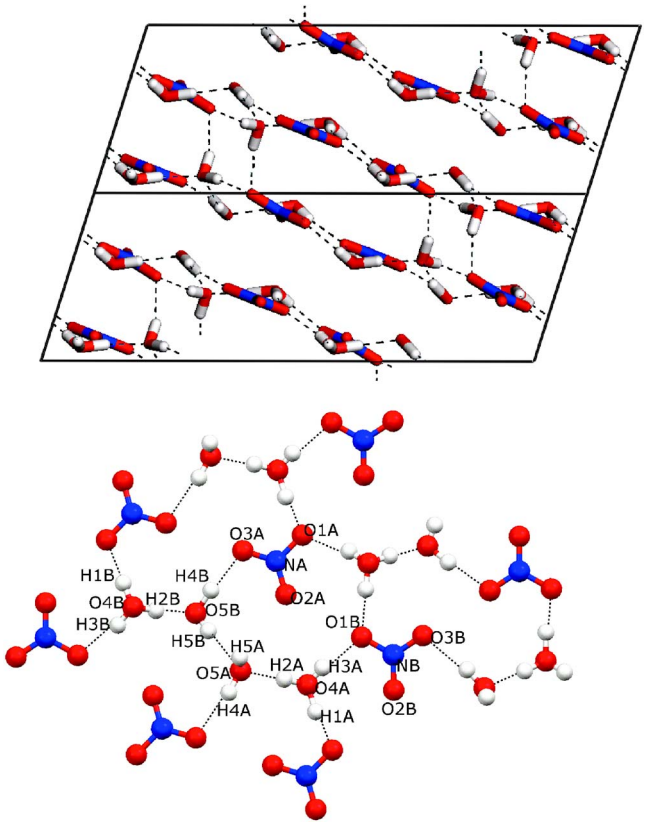

FIG. 2. (Color online) Crystal structure of phase I NAD (above) and connectivity map (below).

A number of computational and experimental studies on NAD have been published. Escribano *et al.*[10] and Fernández *et al.*[11] initially studied a gas phase structure (i.e., isolated cluster) and found (at cc-pVTZ, B3LYP) the $HNO_3 \cdot 2H_2O$ moiety to be of lower energy, compared to the ionic form $[NO_3]^- \cdot [H_3O]^+ \cdot H_2O$. This study was followed by simulations using localized/pseudopotential basis sets with density functional theory (DFT) and periodic boundary conditions,[11] which showed that in the solid phase $[NO_3]^- \cdot [H_3O]^+ \cdot H_2O$ was the more stable structure. Both studies produced calculated vibrational spectra. Comparison with experiment[12] shows that the gas phase calculations are not an appropriate representation for solid-state NAD, as they overestimate some modes by approximately 500 cm^{-1}. This is to be expected as large amplitude, strongly anharmonic vibrations are misrepresented by the harmonic approximation, coupled to the fact that the gas phase cluster is, in any case, a poor representation of the solid. Calculations performed with periodic boundary conditions fared much better, accurately reproducing the majority of vibrations to within a few wave numbers. However, some vibrations appear to be misrepresented, with, for example, the $[H_3O]^+$ symmetric stretch experimentally reported[13] to be in the region of 2714 cm^{-1} but calculated to be 2982–3017 cm^{-1}, and no frequencies are calculated less than 1000 cm^{-1}. The clear improvement can be attributed to the superior model, as the periodic boundary conditions better reflect the repeating unit of the crystal. However, as the vibrational frequencies were based on atomic Cartesian displacements (i.e., a harmonic oscillator), there is still room for improvement.

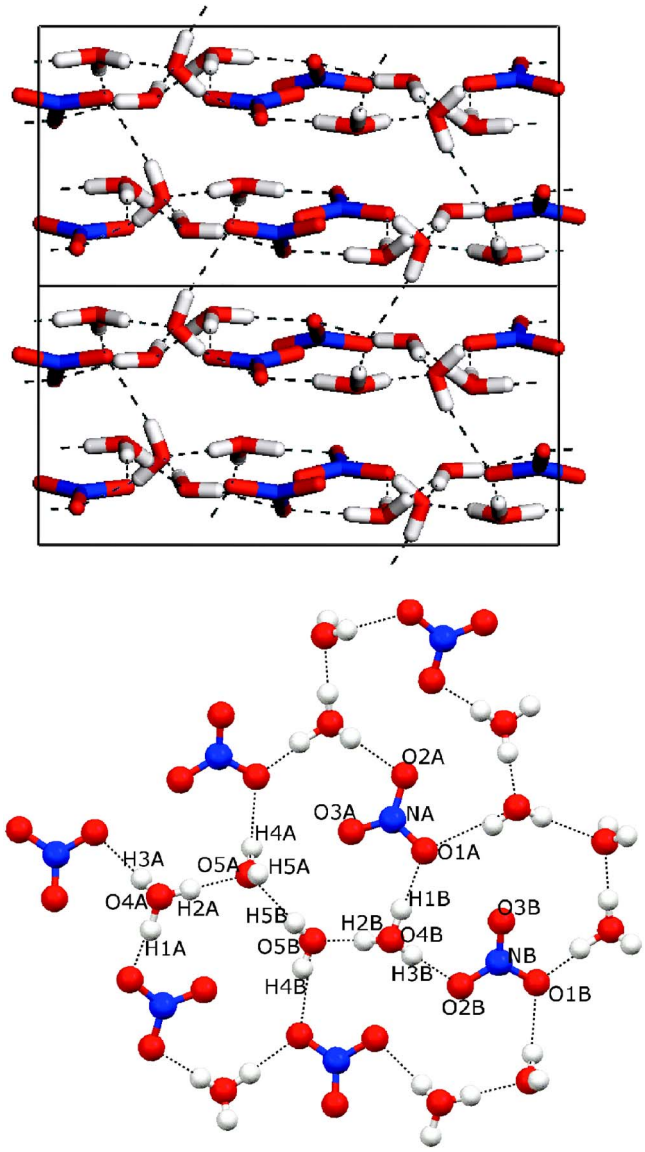

FIG. 3. (Color online) The crystal structure (above) and layer system (below) adopted by phase II of phase II NAD (above).

In the NAD crystal structure, proton transfer occurs from the nitric acid to one of the water molecules, thus creating a unit cell containing $[NO_3]^-$, $[H_3O]^+$, and H_2O. Identifying the oxonium anion and water molecule sites in a high pressure x-ray diffraction experiment is a considerable challenge. The sample is mounted in a diamond-anvil pressure cell, the nature of which restricts the volume of reciprocal space that can be accessed. The data set is not only more restricted than that collected from a conventional ambient pressure study, but the intensity statistics of the reflections are also generally poorer. Consequently, the hydrogen atom positions are usually not determined in the crystal structures. *Ab initio* modeling can, however, be applied to complete the structure. While Monte Carlo (MC) simulations are often applied in similar situations, the partially complete structure offered by experiment allows more computationally intense simulations to be used. Specific to this case, standard (i.e., modeling based on classical physics), modeling techniques can prove

inaccurate when studying the protonated water dimer ion $[H_5O_2]^+$.

Completing the structure computationally is essentially a straightforward task: The unit cell parameters and heavy-atom positions are supplied by experiment and the input model completed with approximate hydrogen atom positions. The crystal structure is then optimized quantum mechanically in order to find the lowest energy atomic arrangement. Treating structures in this manner can create a problem, in that the geometry optimization algorithm will only minimize the structure to the nearest local energy well, and there is no guarantee that this minimum represents the lowest energy structure on the potential energy surface. Through our earlier study of nitric acid monohydrate at high pressure, we developed a computational procedure involving molecular dynamics (MD) calculations to more fully probe the local energy surface, and thus raise confidence levels on the hydrogen atom positions obtained.[6]

While this method successfully obtained complete structures for three different polymorphic phases of nitric acid monohydrate, the dihydrate derivative is a much more challenging case. In addition to the problem of identifying the $[H_3O]^+$ and H_2O sites, there exists the possibility that proton transfer can occur between these two molecules. The protonated water dimer $[H_5O_2]^+$ has been extensively studied due to its pivotal role in proton transfer in aqueous solutions[14] and so-called water wires.[15] However, this interesting ion presents several problems when studied from a theoretical perspective: A large flat potential energy surface presents convergence issues, and large amplitude, strongly anharmonic vibrations means the harmonic approximation will not accurately represent the vibrational modes. Finally, the possibilities for low energy rearrangement pathways generate multiple conformer issues. In our calculations we are able to sample the flat nature of the minimum by performing MD simulations, thereby allowing more of the potential energy surface to be taken into account than would be possible by geometry optimization alone, and would also allow any structural rearrangements due to skipping into other nearby energy wells to be observed. In addition, the vibrational frequencies we extract from our MD simulations are automatically corrected for anharmonic effects. Finally, we can run a series of single point energies along a given trajectory to explore and visualize the potential energy surface. Our methods of computational analysis are therefore ideally suited to allow meaningful study of the $[H_5O_2]^+$ ion within the crystal lattice.

In this paper we report on *ab initio* calculations on the previously known ambient pressure polymorphs of nitric acid dihydrate. Also reported is a new phase recorded using high pressure crystallographic techniques. The initial structure was obtained using single crystal x-ray diffraction (3.8 GPa), with quantum mechanical calculations (plane-wave density functional theory, PW-DFT) then being employed to complete the partial experimental structure, thus allowing the hydrogen atom positions to be located with a much greater degree of confidence. This was then followed by a high pressure neutron diffraction experiment on the per-deuterated analogue system, thus allowing the validity of our computational model to be fully assessed. We also report the calculated vibrational spectra for the different structures studied.

EXPERIMENT AND COMPUTATION

High pressure x-ray diffraction

The crystals were grown by loading and pressurizing a 68% (by weight) aqueous solution of nitric acid in a Merrill and Bassett diamond-anvil cell[16] that had been equipped with 600 μm culet diamonds and a tungsten gasket. A 68 wt % solution represents a $HNO_3:H_2O$ ratio of $1:\sim 1.65$ indicating that dihydrate crystallizes preferentially as single crystals over monohydrates and trihydrates (some polycrystalline material was also present presumably due to the 1:1 monohydrate). The $HNO_3:H_2O$ ratio is of little significance for generation of phase III NAD; subsequent experiments have found that ratios favoring a monohydrate crystallize as mixed dihydrate when under pressure. The gasket had been preindented to a thickness of 100 μm and had a 200 μm hole drilled through it. After the nucleation of several crystallites, the temperature was cycled close to the melting curve in order to reduce the number of crystallites, in a manner similar to that of Vos *et al.*[17] Finally, a single crystal was obtained at a pressure of 3.8 GPa. Subsequent pressure increases yielded the high pressure phase of NAD.

The setting angles of strong reflections were determined on an Enraf-Nonius CAD4 diffractometer equipped with a Mo x-ray tube. Following initial indexing, a least squares fit yielded orthorhombic unit cell parameters, listed in Table I. Intensity data were collected with the ω-scan method, at the position of least attenuation of the pressure cell, according to the fixed-ϕ technique. All accessible reflections were measured in the hemisphere $\pm h$, $\pm k$, $\pm l$, for $0\ \text{Å}^{-1} < \sin\theta/\lambda < 0.71\ \text{Å}^{-1}$. The intensities were corrected for absorption, averaged, and then used for structure solution by direct methods.

The systematic absences for phase III NAD were consistent with the $P2_12_12_1$ space group, and an initial trial solution in this symmetry was found to be acceptable. The final structural model was refined using the CRYSTALS suite of programs[18] and the structural parameters to the various fits, along with the refinement statistics, are listed in Table I. The data and crystal quality were sufficient to allow the displacement parameters to be refined anisotropically.

Computational methods

Equilibrium structures for the nitric acid dihydrate series were obtained using the VASP 4.4 simulation package[19] according to the following procedure. Initial geometries and space group symmetry constraints were taken from experiment. In the case of unlocated hydrogen atoms (i.e., the high pressure phase III structure), nominal positions were selected based on a close inspection of the heavy-atom positions and assuming pseudo D_{3h} and C_{2v} structures for the $[H_3O]^+$ ion and H_2O molecule, respectively. A set of atomic position optimizations were performed initially such that a favorable hydrogen bonding network would be in place before any

TABLE I. Crystallographic data for nitric acid dihydrate at elevated pressure.

	Phase I		Phase II		Phase III			
	exp	calc	exp	calc	x-ray	calc (α)	calc (β)	neutron
Space group	$p21/n$	$p21/n$	$p21/n$	$p21/n$	$p212121$	$p1$	$p1$	$p212121$
a (Å)	17.509(3)	17.431	9.674(3)	9.683	9.391(7)	9.483	9.458	9.4573(15)
b (Å)	7.619(4)	7.660	12.920(4)	12.944	3.127(2)	6.453[a]	6.518[a]	3.1776(3)
c (Å)	6.253(3)	6.382	6.484(3)	6.563	11.253(9)	11.294	11.211	11.3124(18)
$\alpha=\gamma$	90	90	90	90	90	90	90	90
β	107.5(3)	108.631	97.71(3)	97.71	90	90	90	90
Volume (Å^3)	796(2)	807.545	803(1)	815.88	330.5(4)	691.2	694.3	340.0(9)
Z	8	8	8	8	4	8	8	4

[a]Note $1\times2\times1$ simulation cell used for phase III structure.

volume change was permitted. This was then followed by a series of single-point energy calculations where the lattice constants (multipliers for the cell vectors) were varied, thus establishing the volumes of the unit cells that gave rise to the lowest energies. All subsequent optimizations were then held at these fixed volumes. The atomic positions and lattice parameters were then optimized on alternate cycles, until convergence was achieved. Phase III NAD calculations were performed using two different models (in $P1$ symmetry using a $1\times2\times1$ supercell), corresponding to the two possible likely geometries for the $[H_3O]^+$ ion and H_2O molecule. For all other phases, a $1\times1\times1$ (i.e., crystallographic) cell was used, and the appropriate symmetry constraints applied. Simulations were performed using a set of ultrasoft pseudopotentials[20] and plane waves expressed at an energy cutoff at 396 eV. The generalized gradient approximation (GGA) functional PW91 (Ref. 21) was used to model the exchange and correlation potentials, and the Brillouin zones sampled by one k point at the gamma (Γ) position. Convergence criteria were set such that optimization was achieved once forces reached less than 10^{-3} eV Å^{-1} and self-consistent field results (SCF) energy less than 10^{-4} eV.

The equilibrium structure work was then followed by a series of PW-DFT microcanonical (NVE) molecular dynamics calculations performed in the $P1$ space group, in order to search the potential energy surface more completely, and to investigate the effects of temperature (i.e., free energy) on the resulting thermally averaged structures. This also offered the opportunity to extract solid-state vibrational frequencies from the simulation by Fourier transformation of the autocorrelation function of the calculated forces, with low frequency noise subtracted from the resulting spectra using a Blackman windowing function.[22] Here, the basis set energy cutoff was lowered to 297 eV, and identical convergence criteria and k point sampling as for the equilibrium calculations were used. With the equilibrium structures used as starting points, MD simulations were run using a time step of 0.7 fs, determined after careful consideration of the highest energy vibrational frequency for the system (the O–H stretch). Confirmation of this time step was obtained by analysis of the resulting conservation of free energy in the NVE ensemble. The first 0.14 ps of each simulation was discarded to allow the system to reach equilibrium; data collection was then accrued over a further 0.7 ps. The temperatures for phase I, phase II, and phase III averaged to 243 K, 220 K, and 218 K, respectively. A second simulation was subsequently performed on the phase I structure with a lower average temperature of 77 K.

Scans of the potential energy surfaces were obtained by taking the relevant O···O vectors and assuming a minimum O–H distance (around 0.9 Å); the remaining length $[r(O\cdots O)-2r(O-H)]$ was divided into nine equal fractions. Initial scans were obtained from single point energy calculations with the hydrogen positioned at each fraction along the O···O vector (Fig. 6). This was then followed by a second scan where the atomic positions were allowed to relax, with the exception of the two bridging oxygen atoms, which were fixed at their equilibrium geometry positions.

High pressure neutron diffraction

High pressure neutron powder diffraction data were collected for $DNO_3\cdot(D_2O)_2$ using the PEARL/HiPr diffractometer[23,24] at the U.K. spallation neutron source, ISIS, located at the CCLRC Rutherford Appleton Laboratory. A solution ($\sim$100 mm^3) of composition $\sim$1:1 was added to a TiZr capsule gasket[25] filled with loosely packed powdered silica wool that was used to inhibit the formation of large crystallites. A small pellet of aluminum foil was also added to act as a pressure marker. The resulting capsule assembly was then compressed within a type V3b Paris-Edinburgh (P-E) pressure cell[26,27] equipped with standard single toroid anvils with cemented WC cores (Ni binder). The P-E cell ram pressure was monitored and controlled by means of a computer-controlled hydraulic system. The experiment was conducted without the use of a pressure transmitting medium due to the chemically aggressive nature of the sample. As such, the maximum useful pressure was limited to $\sim$4 GPa by the onset of diffraction peak broadening resulting from nonhydrostatic stress within the sample.

Time-of-flight (TOF) neutron powder diffraction data suitable for structure refinement were obtained by electroni-

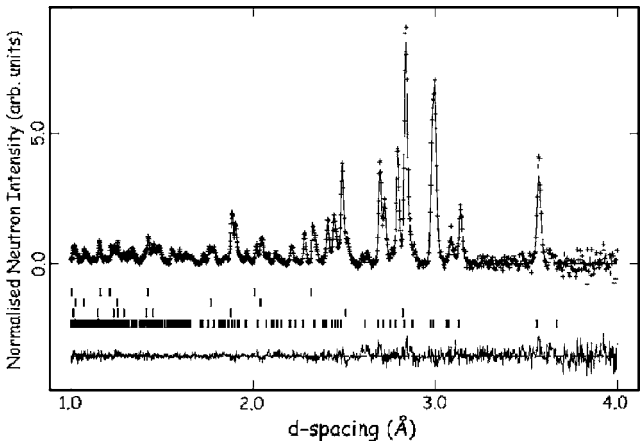

FIG. 4. Powder diffraction pattern at 26 tons loading, with Al and silica wool.

cally focusing the 1080 individual detector element spectra of the main PEARL/HiPr $2\theta=90°$ detector bank. The summed pattern was then normalized with respect to the incident beam monitor and the scattering from a standard vanadium calibration sample. Last, the diffraction pattern intensities were corrected for the wavelength and scattering-angle dependence of the neutron attenuation by the P-E cell anvil (WC) and gasket (TiZr) materials[28] (see Fig. 4 for powder diffraction pattern). Typical data collection times were 6 h at full ISIS beam, which equates to an integrated proton current of ~1 mA/h. Full-profile Rietveld refinements of the TOF neutron powder diffraction patterns were carried out using the GSAS package.[29] Sample pressures were calculated from the refined Al lattice parameters and the known room-temperature equation of state.[30]

RESULTS AND DISCUSSION

Phase I

Following a straightforward optimization procedure, the resulting (calculated) equilibrium structure compared well with that obtained experimentally (see Table II), with the majority of heavy-atom distances reproduced to within 0.03 Å and a minimal volume increase [1.5%, as current DFT functionals cannot calculate dispersion forces (i.e., van der Waal interactions) some volume expansion is nearly always expected within the GGA formulism]. Visual superposition of the two structures confirmed that the calculated minimum corresponded well with that obtained from experiment. We can therefore conclude that the computational approach is capable of reproducing the key features of the nitric acid dihydrate structure.

In order to further explore the potential energy surface (PES), a molecular dynamics (MD) calculation was then undertaken with the temperature equilibrated at approximately 200 K. This allowed direct visualization of the flexibility of the system and any local wells to be accessed if the system has enough thermal energy to overcome any potential energy barriers. Visualization of the MD simulation showed that despite the lack of symmetry constraints a pseudo $P2_1/n$ space

TABLE II. Phase I heavy-atom distances. For atom numbering, see Fig. 2.

	Phase I Distances (Å)	
	exp	calc
N-O2 (*A*)	1.222(2)	1.244
N-O2 (*B*)	1.223(2)	1.240
N-O3 (*A*)	1.235(2)	1.265
N-O3 (*B*)	1.253(2)	1.277
N-O1 (*A*)	1.286(2)	1.301
N-O1 (*B*)	1.279(2)	1.301
O1A-O4A	2.550(2)	2.576
O1B-O4B	2.606(2)	2.630
O1A-O4B	2.628(2)	2.635
O1B-O4A	2.604(2)	2.592
O3A-O5B	2.768(2)	2.719
O5A-O3B (interplane)	2.940(2)	2.827
O3B-O5A	2.828(2)	2.778
O4A-O5A	2.559(2)	2.551
O4B-O5B	2.460(2)	2.422

group was retained; furthermore, the main geometrical features were still present. The hydrogen positions, however, showed some interesting behavior. The type 1 $[H_5O_2]^+$ ion, [O4A-H2A-O5A, see Fig. 1(a) and Fig. 2] has O–H and H···O distances of 0.93(2) and 1.64(2) *Å*, respectively, compared to calculated distances of 1.041 and 1.510 Å. This reflects the typical underestimation of O–H bond lengths by x-ray diffraction. The heavy atom O···O distances showed a much smaller deviation: experiment 2.559(2) *Å*, calculated 2.560 Å. The hydrogen bonds linking $[H_3O]^+$ to H_2O, which are crystallographically in a layer {i.e., $[H_5O_2]^+$ type 2, O4B-H2B-O5B, see Fig. 1(b) and Fig. 2}, have O–H···O distances of 0.91(3) and 1.55(3) *Å* respectively; in the calculated equilibrium geometry distances of 1.146 and 1.275 Å were determined. The heavy-atom structure remained close to that obtained experimentally, with the O4B···O5B distance recorded at 2.460(2) and 2.422 Å by experiment and theory, respectively. This rather short heavy-atom bond distance, is indicative of a "strong" hydrogen bond.[31] The shape of the PES for strong hydrogen bonds tends to be a broad flat single well, which potentially allows the phenomenon of proton migration to occur. When kinetic energy is added to the system (i.e., the MD simulation), we indeed observe the bridging hydrogens shuttling between O4B and O5B, and upon averaging remaining close to equidistant from both oxygens. After the hydrogen shuttling, no further phase changes were observed from this simulation.

In order to explore the behavior of the shuttling hydrogen bridge further, a second MD simulation was performed at a lower temperature (~80 K). This calculation also sought to alleviate the concern that the equilibrium temperature for the phase I MD simulation was above that at which the phase II structure is observed experimentally. It was also believed that, should the temperature drop sufficiently, the mobility of

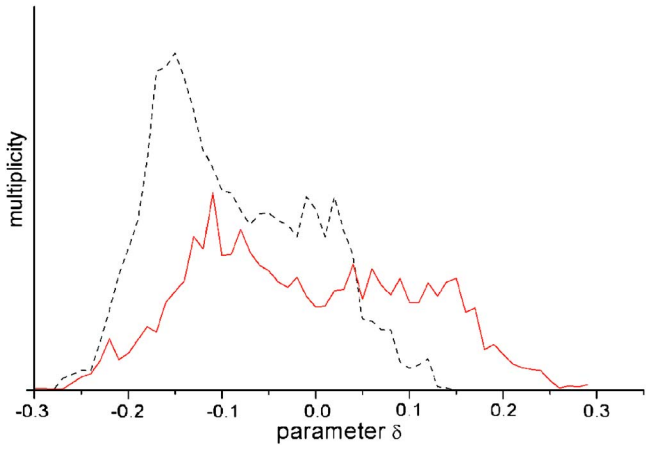

FIG. 5. (Color online) Delta parameter plots; a negative value represents the bridging hydrogen lying closer to O4B, positive to O5B. Solid line represents high temperature (243 K) MD, dashed line represents the low temperature MD (77 K).

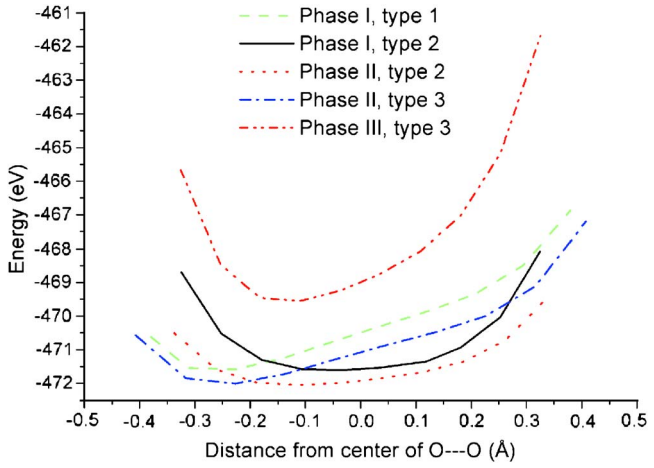

FIG. 6. (Color online) Single point energy potential energy surfaces, phase I type 2 is the only conformation of the $[H_5O_2]^+$ ion that exhibits proton shuttling behavior.

the hydrogen atom would be reduced such that it associates with just one water molecule. To quantify the degree of proton shuttling observed in the two MD simulations, we define a parameter labeled δ, which denotes the deviation of the hydrogen atom from the center of the O···O vector. A value of zero indicates the bridging atom lies exactly in the middle of the bond, a negative value that the proton lies closer to O4B, positive O5B. A multiplicity plot of δ (expressed to two decimal places) averaged over all $[H_5O_2]^+$ type 2 ions in the unit cell for both MD runs is shown in Fig. 5. As the temperature decreases, it is clear that the hydrogen tends to locate more on one of the oxygen atoms (O4B) than the other. The equilibrium temperature for this simulation ($\sim$80 K), is much lower than the conditions under which the phase was observed experimentally (225 K). Note, however, that even at the lower temperature the hydrogen does show some propensity towards shuttling. The fact that this was not observed experimentally is not surprising. The hydrogen atom is difficult to observe experimentally using x-ray diffraction; therefore, in all likelihood, a variable temperature neutron diffraction study would be required to enable the temperature evolution of the hydrogen atom position to be fully observed.

To visualize the nature of the potential energy well for this O···H···O type 2 interaction, PES scans were performed. The bridging hydrogen atom was transported along the O···O vector in a set of nine increments from an initial O(4B)–H distance of 0.882 to an H···O(5B) distance of 0.882 Å, assuming a linear OHO moiety. Initially the PES was generated from a series of single point energy calculations, with all other atoms fixed at the equilibrium geometry. The results are presented in Fig. 6. This was then followed with a second PES scan where all atoms (except the oxygen and hydrogen atoms directly involved in the short hydrogen bond) were allowed to optimize, allowing a mode softening to occur with the general shape of the PES remaining. While this approximation is rather crude (a more accurate PES could be obtained from a multidimensional parameter scan, where the OH distance is varied with the OHO angle and the O···O vector, but the large number of steps required renders this calculation impractical). Since the general shape of the PES remained unchanged by these, more elaborate, calculations, they were not pursued beyond that of a test on phase I type 1, which is not recorded in Fig. 6. The general shape of the PES can be observed and some explanation can be inferred as to why the phase I type 2 dihydronium ion conformation exhibits proton shuttling while the other conformations do not. Although the potential well around H2B showed the traits indicative of a shuttling hydrogen (large flat minimum), other potential surfaces appeared to be tilted, as to favor a single hydrogen site. However, it must be noted that the potential energy surfaces we calculate are derived from pure DFT calculations, and as such are expected to underestimate any barrier heights that may be present (indeed, specific to this work is the study by S. Sadhukhan *et al.*[32] on the $[H_5O_2]^+$ cation, which showed that the pure DFT functionals BLYP and PBE underestimate a gas phase barrier height by up to 3.0 kcal mol^{-1}). The issue of whether or not the shuttling phenomenon we observe in our MD simulation of the phase I structure of NAD is a genuine or artificial effect could be resolved by neutron diffraction, and this is work we will undertake shortly.

From the MD simulation a predicted vibrational spectrum may be produced, based on an autocorrelation of the forces obtained at each step. Whilst formal identification of each mode is not straightforward, as with normal mode analysis, performing the Fourier transform for selected atoms allows us to block out regions of the spectra for the different elements present. Hence vibrations involving the hydrogen atoms can be observed occurring at 2450–3610 cm^{-1}, whilst vibrations due to nitrogen are located between 650 and 1400 cm^{-1} and oxygen vibrations occur across the full range of the spectrum. The predicted vibrational spectra of NAD I (Fig. 7) repeats many of the details shown in the experimental spectra,[13] with broad intensities roughly where broad intensities are expected. As with all reported spectra in this paper, peak intensities do not translate to spectral intensities (i.e., are not weight averaged). It is worthy of note that obtaining experimental solid-state spectra of the hydrated nitric

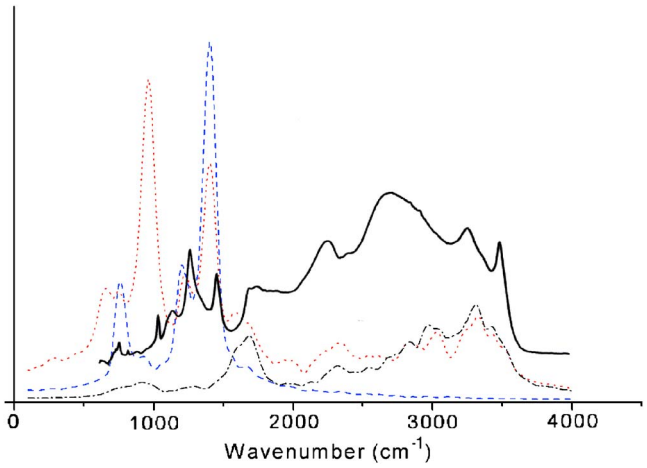

FIG. 7. (Color online) Vibrational spectra of NAD I; oxygen vibrations dotted, nitrogen vibrations dashed, hydrogen vibrations dot-dashed. An experimental IR comparison (Ref. 13) is included as a solid line.

acid species is no simple matter, as all the separate hydrate species are likely to be present. However, with the aid of x-ray crystallography, Tizek *et al.*[12] are confident in their reported IR spectral assignment. With the exception of the $[NO_3]^-$ symmetric stretch (930 cm^{-1}), which is not IR active (and hence not present on the experimental spectrum), the predicted and experimental spectra show good correlation.

Phase II (225 K)

The experimental study of this phase also reported all atomic positions with a high degree of accuracy, which again allowed us to carefully check the quality of our simulations. Like the phase I structure, the optimization procedure was straightforward. The main structural features were retained (Table III), indicating that the computational approach used to model this system was appropriate and could be extended to the work at high pressure, where much less of the structure is known from our x-ray diffraction measurements. To search for possible similar proton-migrating phenomena as occurred in phase I, and to correct for possible problems originating from the troughlike nature of the PES, a full MD simulation was performed, allowing a complete assessment of structural changes resulting from an increase in temperature.

The two $[H_5O_2]^+$ geometries present in this structure are of types 2 and 3, which differs from phase I which contains type 2 and the lowest energy dihydronium conformation type 1. Interestingly, although this higher temperature polymorph contains the same dihydronium unit that displayed proton shuttling in the phase I structure (type 2), no migratory effect was observed in our molecular dynamics simulation. Performing a PES scan similar to that of phase I (i.e., stepping the *r*O–H distance from 0.919 to 1.527 Å in nine incremental steps, with all other atoms fixed at equilibrium positions) produces a similarly shaped potential energy well as observed for the type 2 unit in phase I, but the bottom of the well is slightly tilted, thus favoring a single hydrogen location (Fig. 6).

TABLE III. Phase II heavy-atom distances. For atom numbering see Fig. 3.

	Phase II Distances (Å)	
	exp	calc
N-O2 (*A*)	1.214(4)	1.239
N-O2 (*B*)	1.227(4)	1.234
N-O3 (*A*)	1.265(4)	1.265
N-O3 (*B*)	1.246(4)	1.288
N-O1 (*A*)	1.263(4)	1.287
N-O1 (*B*)	1.278(4)	1.277
O1A-O4B	2.640(4)	2.633
O1B-O4A	2.521(4)	2.581
O1A-O5B	2.832(4)	2.809
O1B-O5A	2.827(4)	2.789
O2A-O4A	2.626(4)	2.601
O2B-O4B	2.663(4)	2.623
O5A-O2A (interplane)	2.884(4)	2.792
O4A-O5A	2.553(4)	2.547
O4B-O5B	2.459(4)	2.466

The MD-extracted vibrational spectrum (Fig. 8) repeats many of the characteristics of the previous phase: a broad O–H region, sharp O–N vibrations. The broad nature of many of the vibrations makes characterization difficult. Comparing the experimental spectra[13] with that calculated indicates many similarities; showing broad absorptions from approximately 3500 cm^{-1} to 1700 cm^{-1} and sharper absorptions below 1700 cm^{-1}. The accuracy of the simulation adds credence to the ability of PW-DFT calculations to model this system.

From our modeling studies of the ambient pressure phases of nitric acid dihydrate, we conclude that PW-DFT has successfully reproduced the key geometric features of the two previously known phases. We now turn to the high pressure

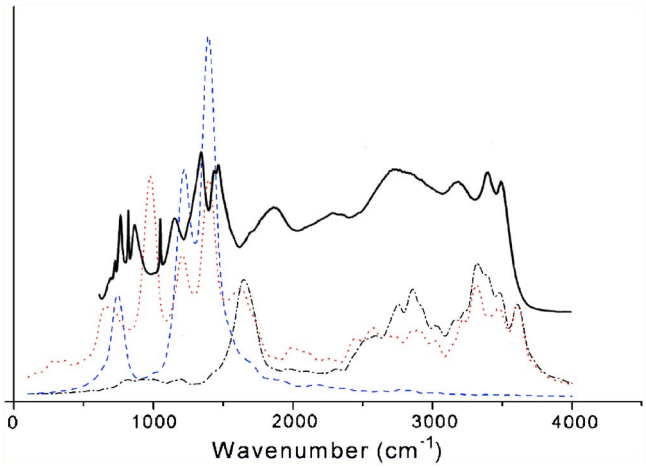

FIG. 8. (Color online) Vibrational spectra of NAD phase II; oxygen vibrations dotted, nitrogen vibrations dashed, hydrogen vibrations dot-dashed. An experimental IR comparison (Ref. 13) is included as a solid line.

TABLE IV. Phase III heavy-atom distances. For atom numbering see Fig. 9.

	Phase III Distances (Å)		
	x-ray	calculated	neutron
N-O2	1.252(13)	1.268	1.245(9)
N-O3	1.252(12)	1.248	1.250(9)
N-O1	1.240(18)	1.288	1.240(9)
O1-O5	2.692(15)	2.666	2.717(22)
O1-O4	2.576(11)	2.592	2.623(22)
O2-O4	2.664(18)	2.608	2.725(21)
O3-O5	2.924(14)	2.951	2.925(23)
O4-O5	2.448(15)	2.451	2.370(21)
O5-D3	—	1.367	1.377(21)
O1-D4	—	1.627	1.820(21)
O3-D5	—	2.096	2.128(20)
O1-D1	—	1.574	1.661(21)
O2-D2	—	1.604	1.745(21)

TABLE V. Experimental and calculated lattice parameters for the three phases of NAD.

Pressure (GPa)	3.8
Crystal system	Orthorhombic
Space Group	$P2_12_12_1$
No. reflections for cell	17
$2\theta_{max}(^\circ)$	80
Z	4
Reflections collected	843
No. Unique [R_{merge}]	394 [0.052]
No. $F>4u(F)$	278
Parameters	25
R_1 [$F>4u(F)$]	0.1151
wR_2 (F, all data)	0.0355
S	1.209
$\Delta\rho_{max}$ (eÅ^{-3})	0.66
$\Delta\rho_{min}$ (eÅ^{-3})	–0.42

structure, where our initial experimental measurements were unable to locate the positions of the hydrogen atoms. As a consequence, the nature of the dihydronium ion is undetermined for this phase, presenting an interesting modeling challenge for this previously unknown structure.

Phase III (3.8 GPa, 273 K)

High pressure x-ray diffraction

The heavy-atom structure obtained by single crystal x-ray diffraction was found to be of orthorhombic $P2_12_12_1$ symmetry with a unit cell volume less than half the size of the ambient pressure cells (see Table IV). The asymmetric unit of phase III NAD contains one $[NO_3]^-$ and one $[H_5O_2]^+$ ion, unlike the previous two phases that contained two $[NO_3]^-$ and two $[H_5O_2]^+$ ions. As this initial x-ray study could not locate hydrogen atom positions, we are unable to distinguish between the $[H_3O]^+$ and H_2O sites, and also whether the dihydronium unit is of type 1, 2, or 3. Input was therefore required from quantum mechanical calculations and/or neutron diffraction to complete the structure. In this study we were fortunate to be able to do both. We undertook a computational investigation first in order to complete the x-ray diffraction refinement; this in turn provided a complete set of atomic positions as a starting model for the neutron diffraction study. A successful refinement of the neutron diffraction data would therefore validate our computational result.

Computation

The x-ray diffraction study provided a set of starting parameters for the unit cell and heavy-atoms positions. As the $[H_3O]^+$ and H_2O sites were indistinguishable from the experimental study, two models were constructed, labeled α and β, where the two sites were interchanged. The $[H_3O]^+$ ion was started from a planar, pseudo D_{3h} geometry (to prevent artificially favoring a particular structure) and the H_2O molecule from pseudo C_{2v} local symmetry. Initial geometry optimizations of both models, however, yielded poor results, with unreasonable lattice parameters and large heavy-atom displacements. Large displacements arise in systems where one (or more) axis is much less than either of the others, due to the relative pressures exerted on each axis (smaller area =higher pressure); this problem can be resolved by doubling up to a supercell along any small axis.[7] Further calculations performed with $1\times2\times1$ supercells helped stabilize both models, reducing heavy-atom displacements to acceptable levels, with the majority of heavy-atom distances reproduced to within 0.04 Å and minimal volume increases (4.6%) in both cases (Tables IV and V). Despite the removal of all symmetry constraints, the structure maintained a pseudo $P2_12_12_1$ space group throughout the simulation.

The two models produced equilibrium geometries of similar energies (α=469.77995 eV and β=469.77255 eV), but with nonidentical structures, each corresponding to the initial dihydronium ion conformation. Both of these structures were studied with MD simulations, allowing the hydrogen to shuttle, and hence a possible transition between the two structures may be observed. Model β, however, showed instabilities in the MD simulation, with large unrealistic displacements in the nitrate ion positions. Model α, on the other hand, appeared to be much more robust. On this basis, model β was eliminated as a possible geometry, and the coordinates obtained for the optimized structure of model α (Fig. 9) put forward as a starting model for the high pressure neutron diffraction study refinement.

The dihydronium ion thus found in the simulation is of type 3 and shows no proton migration. A PES scan was performed to determine why this was, which indicated that the floor of the well appears to be tilted favoring just one hydrogen atom location (see Fig. 6). Hydrogen atom migration therefore seems unlikely for this structure even at elevated temperatures.

The predicted vibrational spectra (Fig. 10) displayed fewer, better defined peaks relative to phases I and II, which

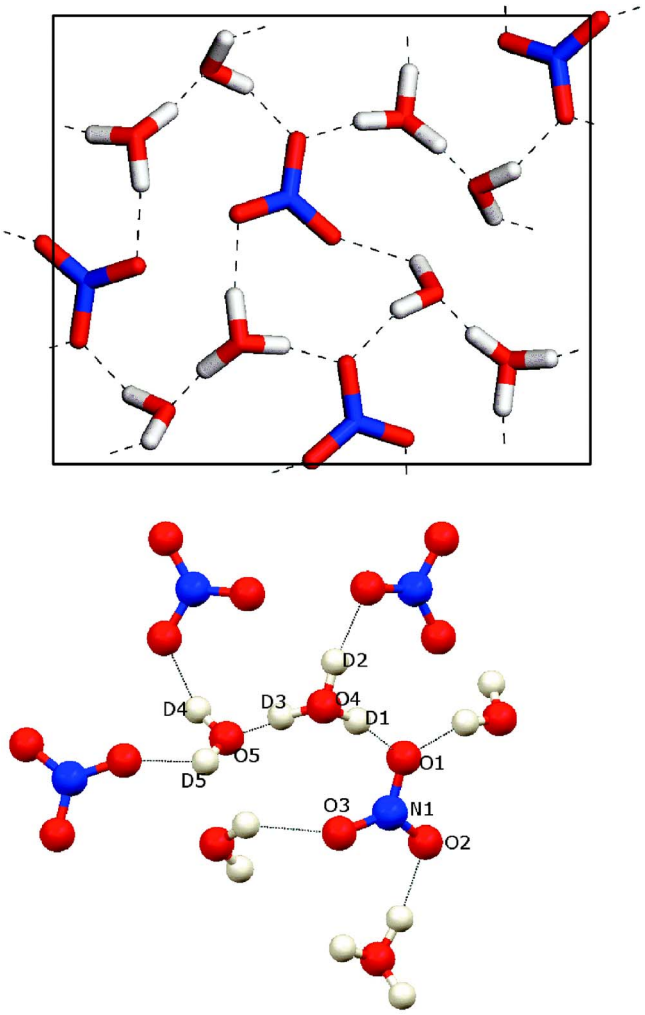

FIG. 9. (Color online) crystal structure of NAD phase III (above) and connectivity map (below).

can be attributed to the smaller asymmetric unit of the phase III structure.

High pressure neutron diffraction

Following the high pressure neutron diffraction technique, phase III NAD was first observed at 1.33 GPa. Since simulations yielded promising results identifying hydrogen locations, the 0 K equilibrium structure was used as the model for refinement. Differences in pressure and the isotopic substitution can account for small differences, but on the whole only minimal displacements are expected. The structure determined by neutron diffraction (Table IV) was remarkably close to that predicted by simulation, confirming the α model as the optimal structure.

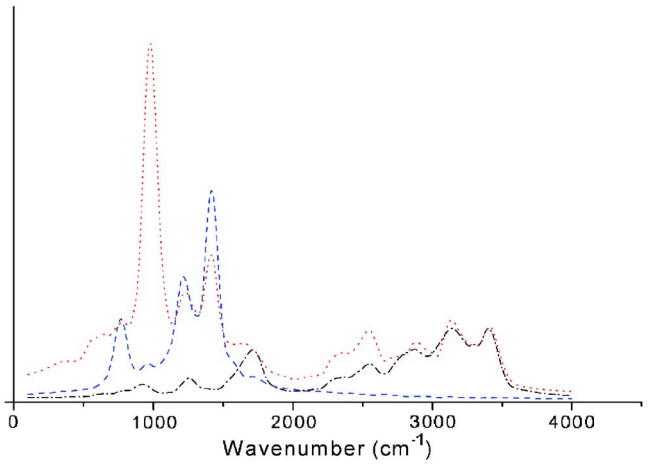

FIG. 10. (Color online) Vibrational spectra of high pressure NAD phase III; oxygen vibrations dotted, nitrogen vibrations dashed, hydrogen vibrations dot-dashed.

CONCLUSIONS

Three nitric acid dihydrate species have been studied computationally. A new high pressure phase was initially observed and characterized by x-ray diffraction and computational means, and the completed crystal structure proposed was later confirmed by neutron diffraction. The dihydronium ions present in each dihydrate are observed to form in three geometries. One of these—type 2 [Fig. 1(b)]—shows the interesting feature of a shuttling hydrogen present in a short O···O linkage. This interesting phenomenon is easily overlooked experimentally, due to hydrogen having a minimal scattering density to diffract x-rays. While the same conformation of the dihydronium ion is found on two other occasions (phases 1 and 2), the phenomenon of proton shuttling is observed in our MD simulations only once, indicating the sensitivity of the shuttling hydrogen to external potentials. Further work is required to fully examine this effect.

ACKNOWLEDGMENTS

We thank EPSRC and the University of Edinburgh (School of Chemistry) for funding. CAM acknowledges support from the Royal Society, and DRA the EPSRC and CCLRC for access to neutron diffraction facilities. This work was carried out using computational facilities supplied by EPCC at the University of Edinburgh.

[1] M. J. Molina, T.-L. Tso, L. T. Molina, and F. C.-Y. Wang, Science **238**, 1253 (1987).
[2] G. Tóth, J. Phys. Chem. A **101**, 8871 (1997).
[3] D. Salcedo, L. T. Molina, and M. J. Molina, J. Phys. Chem. A **105**, 1433 (2001).
[4] J. J. Marti and K. Mauersberger, J. Phys. Chem. **98**, 6897 (1994).
[5] N. Lebrun, F. Mahe, J. Lamiot, M. Foulon, J. C. Petit, and D. Prevost, Acta Crystallogr. **B57**, 27 (2001).
[6] N. Lebrun, F. Mahe, J. Lamiot, M. Foulon, and J. C. Petit, Acta Crystallogr. **C57**, 1129 (2001).
[7] M. Walker, C. A. Morrison, and D. R. Allan, Phys. Rev. B **72**, 224106 (2005).

[8] G. Zundel and H. Metzger, Z. Phys. Chem. **58**(5/6), 225 (1968).
[9] J. Dai, Z. Bačić, X. Huang, S. Carter, and J. M. Bowman, J. Chem. Phys. **119**, 13 (2003).
[10] R. Escribano, M. Couceiro, P. C. Gómez, E. Carrasco, M. A. Moreno, and V. J. Herrero, J. Phys. Chem. A **107**, 651 (2003).
[11] D. Fernández, V. Botella, V. J. Herrero, and R. Escribano, J. Phys. Chem. B **107**, 10608 (2003).
[12] H. Tizek, E. Knözinger, and H. Grothe, Phys. Chem. Chem. Phys. **4**, 5128 (2002).
[13] H. Grothe, C. E. Lund Myhre, and H. Tizek, Vib. Spectrosc. **34**, 55 (2004).
[14] N. Agmon, J. Mol. Liq. **73&74**, 513 (1997).
[15] N. Agmon, Chem. Phys. Lett. **244**, 456 (1995).
[16] L. Merrill and W. A. Bassett, Rev. Sci. Instrum. **45**, 290 (1974).
[17] W. L. Vos, L. W. Finger, and R. J. Hemley, Nature (London) **358**, 46 (1992).
[18] P. W. Betteridge, J. R. Carruthers, R. I. Cooper, K. Prout, and D. J. Watkin, J. Appl. Crystallogr. **36**, 1487 (2003).
[19] G. Kresse and J. Furthmueller, Comput. Mater. Sci. **6**, 15 (1996).
[20] D. Vanderbilt, Phys. Rev. B **41**, 7892 (1990).
[21] J. P. Perdew, J. A. Chevary, S. H. Vosko, K. A. Jackson, D. J. Singh, and C. Fiolhais, Phys. Rev. B **46**, 6671 (1992).
[22] In-house code following accepted literature practice (M. P. Allen and D. J. Tildesley, computer simulation of liquids).
[23] PEARL (Pressure and Engineering Research Line). ISIS 97, ISIS Facility Annual Report 1996–97 (Rutherford Appleton Laboratory, Oxfordshire, England, 1997), Vol. RAL-TR-97-050, 28.
[24] Dedicated facility for high pressure diffraction. ISIS 96, ISIS Facility Annual Report 1995–96 (Rutherford Appleton Laboratory, Oxfordshire, England, 1996), Vol. RAL-TR-96-050, 61.
[25] W. G. Marshall and D. J. Francis, J. Appl. Crystallogr. **35**, 122 (2002).
[26] R. J. Nelmes, J. S. Loveday, R. M. Wilson, J. M. Besson, S. Klotz, G. Hamel, and S. Hull, *Proceedings of the Symposium on Time-of-Flight Diffraction at Pulsed Neutron Sources*, edited by J. D. Jorgensen and A. J. Schultz, Vol. 29 (American Crystallographic Assoc., Buffalo, 1994), 19.
[27] J. M. Besson, R. J. Nelmes, G. Hamel, J. S. Loveday, G. Weill, and S. Hull, Physica B **180**, 907 (1992).
[28] W. G. Marshall (unpublished).
[29] A. C. Larson and R. B. Von Dreele, Los Alamos National Laboratory Report No. LAUR 2000, 86 (unpublished).
[30] R. G. Greene, H. Luo, and A. L. Ruoff, Phys. Rev. Lett. **73**, 2075 (1994).
[31] G. A. Jeffrey, *An Introduction to Hydrogen Bonding* (Oxford University Press, Oxford, 1997).
[32] S. Sadhukhan, D. Muñoz, C. Adamo, and G. E. Scuseria, Chem. Phys. Lett. **306**, 83 (1999).